Isotopic evidence for two chondrule generations in CR chondrites and their relationships to other carbonaceous chondrites

Yves Marrocchi, Maxime Piralla, Maxence Regnault, Valentina Batanova, Johan Villeneuve, Emmanuel Jacquet

Isotopic evidence for two chondrule generations in CR chondrites and their relationships to other carbonaceous chondrites

Yves Marrocchi[1,*], Maxime Piralla[1], Maxence Regnault[1], Valentina Batanova[2], Johan Villeneuve[1] and Emmanuel Jacquet[3]

[1]Université de Lorraine, CNRS, CRPG, UMR 7358, Vandœuvre-lès-Nancy 54500, France
[2]Université Grenoble Alpes, ISTerre, CNRS, UMR 5275, Grenoble 38000, France
[3]Institut de Minéralogie, de Physique des Matériaux et de Cosmochimie (IMPMC), Muséum national d'Histoire naturelle, Sorbonne Université, CNRS; CP52, 57 rue Cuvier, 75005 Paris, France.

Corresponding author: yvesm@crpg.cnrs-nancy.fr

Abstract

Among primitive meteorites, CR chondrites have peculiar isotopic compositions, the origin of which is uncertain and may have involved contributions from primordial molecular cloud material or the chondrites' formation and agglomeration late during the evolution of the protoplanetary disk. Here, we report a comprehensive textural and isotopic characterization of type I CR chondrules and provide new insights on their formation conditions. We find that two chondrule populations characterized by different sizes and oxygen isotopic compositions co-exist in CR chondrites. The typically larger, ^{16}O-poor ($\Delta^{17}O > -4$ ‰) chondrules (*type I-CR chondrules*) appear to have formed late out of a CR reservoir already populated by typically smaller, ^{16}O-rich ($\Delta^{17}O < -4$ ‰) chondrules (*type I-CO chondrules*). Before formation of *type I-CR* chondrules, the CR reservoir was likely dominated by CI–like dust, in line with the proximity of CR with CI chondrites for many isotopic ratios. The CR reservoir thus may have largely belonged to the continuum shown by other carbonaceous chondrites, although some isotopic ratios maintain some originality and suggest isotopic variation of CI-like dust in the outer disk. Combined with literature data, our data (i) demonstrates that recycling processes are responsible for the singular compositions of CR chondrites and their

chondrules for isotopic systems with drastically different geochemical behaviors (O, Cr, Te) and (ii) support the homogeneous distribution of ^{26}Al throughout the protoplanetary disk.

Keywords: Chondrules, CR chondrites, oxygen isotopes, recycling, protoplanetary disk

1- Introduction

Protoplanetary disks are ubiquitous rotating structures of gas and dust surrounding young stellar objects. They form as a direct consequence of the conservation of angular momentum during the gravitational collapse of dense regions of molecular clouds (Zhao et al. 2020). Although their lifetimes are relatively short (5−10 Ma; Ribas et al. 2015), protoplanetary disks are the sites of phenomenal changes, with solids growing from micrometer-sized particles in the initial molecular clouds to pebbles (centimeters to meters in diameter) and ultimately planetesimals (1–1,000 km in diameter), the main building blocks of planetary bodies (>1,000 km in diameter). Consequently, understanding the chronology and conditions of dust formation in protoplanetary disks is of fundamental importance as they represent the cradles of planet formation.

The early stages of dust growth in the solar protoplanetary disk can be studied by surveying chondrites, primitive rocky meteorites representing fragments of asteroids that never underwent melting. Several studies have revealed that chondrites show a fundamental isotopic dichotomy; carbonaceous chondrites (CCs) are measurably enriched in many neutron-rich isotopes (e.g., ^{48}Ca, ^{50}Ti, ^{54}Cr) compared to non-carbonaceous (NC) chondrites (Kruijer et al. 2017; Trinquier et al. 2007). This dichotomy reflects the formation of their parent bodies in two genetically distinct, contemporaneous, but spatially separated disk reservoirs. The barrier separating the inner (NC) from the outer (C) reservoir has been attributed to the early formation of Jupiter (Kruijer et al. 2017), a long-lived pressure maximum (Brasser and Mojzsis 2020), or evolving ice lines in the disk (Lichtenberg et al. 2021). In this framework, CCs are considered to have accreted at greater heliocentric distances than NCs, consistent with their higher volatile contents (Vacher et al. 2020).

Chondrules, mm-sized igneous spheroids, are the most abundant high-temperature components of both NC and C chondrites, suggesting that both inner and outer solar system reservoirs were affected by their formation. They formed by the solidification of melt droplets interacting with the surrounding gas, although the mechanisms that first produced the droplets remain elusive: they may correspond to melted aggregates of nebular dust or by-products of planetary collisions (e.g., Johnson et al. 2015; Piralla et al. 2021; Tenner et al. 2015). Individual CC chondrules have variable ^{54}Cr excesses (van Kooten et al. 2016, 2020; Olsen et al. 2016; Schneider et al. 2020; Williams et al. 2020; Zhu et al. 2019) whereas NC chondrules display relatively homogeneous ε^{54}Cr, similar to their host chondrites (Schneider et al. 2020; Zhu et al. 2020, 2021). The meaning of ^{54}Cr anomalies in CC chondrules remains debated; they have been ascribed to either (i) variable contribution of ^{54}Cr-rich refractory chondrule precursors (Schneider et al. 2020), such as Ca-Al-rich Inclusions (CAIs, the oldest solids of the Solar System) or (ii) chemical equilibration between ^{54}Cr-poor NC-like chondrules and ^{54}Cr-rich matrix during secondary alteration processes (van Kooten et al. 2021). Furthermore, whether CC chondrules accreted into planetesimals *in-situ* or were transported throughout the disk before their agglomeration also remains debated (van Kooten et al. 2021; Pinto et al. 2021; Schneider et al. 2020; Williams et al. 2020).

Among CCs, metal-rich CR chondrites are of primary importance because they comprise chondrules characterized by higher and less-variable ε^{54}Cr compared to CV, CM and CO chondrites (van Kooten et al. 2016, 2020; Olsen et al. 2016; Schneider et al. 2020; Williams et al. 2020; Zhu et al. 2019). Furthermore, CR chondrites are the only CCs plotting off the δ^{128}Te–ε^{54}Cr mixing line reported for all other CCs (Hellmann et al. 2020) and, along with CH and CB chondrites with which they form the "CR clan", they exhibit isotopically heavy nitrogen and hydrogen (e.g., Aleon 2010). This is generally ascribed to a formation of CR chondrules from different precursor material than other CC chondrules, either because

they formed at larger heliocentric distance (van Kooten et al. 2016, 2020) and/or at later times (Budde et al. 2018; Schrader et al. 2017; Tenner et al. 2019). The wide range of Fe/Mn ratios of type II CR chondrules suggests multifarious origins or at least formation conditions for CR chondrules (Schrader et al. 2015). The nature of CR chondrules' precursors and the specific conditions of the CR chondrule-forming event(s) remain poorly understood. Both of those can be informed by the identification of relict grains surviving from said precursors (e.g., Schrader et al. 2013) and major and minor element zoning controlled by crystal-liquid fractionation and gas-melt exchange (e.g., Libourel and Portail 2018) and also sensitive to oxygen fugacity (Tenner et al. 2018). We are engaged in a systematic study of representative type I (i.e. magnesian, with Mg# = 100×Mg/(Fe+Mg) >90), olivine-rich chondrules by O isotopic measurements by secondary ion mass spectrometry (SIMS) and electron microprobe imaging and analyses in carbonaceous and non-carbonaceous chondrites (Jacquet et al. 2021; Marrocchi et al. 2018, 2019a; Piralla et al. 2021; Regnault et al. 2022). Here, we report a comprehensive study of Mg-rich, type I chondrules in CR chondrites by combining high-resolution cathodoluminescence (CL) maps, electron microprobe analyses, and *in-situ* oxygen isotopic measurements. We use our results to discuss the peculiar formation conditions of CR chondrules and their implications for dust dynamics within the protoplanetary disk.

2- Material and Methods

We surveyed all chondrules within two thick sections of the CR carbonaceous chondrites Renazzo and Dar al Gani 574 (sections no. 719sp3 and 3681sp2, respectively) from the Muséum national d'Histoire naturelle (Paris, France). Both meteorites are listed as CR2 in the Meteoritical Bulletin Database, with Renazzo more precisely classified as CR2.4 in the scheme of Harju et al. (2014). We selected seven type I PO chondrules of different

sizes for further analyses: five from Renazzo and two from Dar al Gani. Apparent chondrule diameters were calculated from the major and minor axes of ellipses fit to BSE images using Adobe Photoshop®. High-resolution CL and quantitative point analyses were performed at the Institut des Sciences de la Terre (ISTerre, Grenoble, France) using a JEOL JXA 8230 electron microprobe equipped with five wavelength-dispersive spectrometers (WDS), a silicon drift detector energy-dispersive spectrometer, and a panchromatic CL system. High-resolution CL maps and fast major-element (Mg, Fe, Si) X-ray maps (on WDS detectors) were acquired simultaneously using an acceleration voltage of 20 kV, a beam current of 100 nA, 1.5-2 μm step size, and a dwell time of 10 ms. This allows the identification of olivine, pyroxene, and glass in chondrules. Quantitative analyses of Al, Ti, Ca, Cr, Mn, Ni, Mg, Fe, and Si in all olivine grains large enough to be isotopically characterized by SIMS were performed with an accelerating voltage of 20 kV, probe current of 900 nA, beam diameter of 1 μm (diameter of interaction volume around 5 μm). The total peak/background counting time was 400 s for Al, Ti, Ca, Mn and 200 s for Cr and Ni with equal counting time in positions of peak and background measured from both sides of the peak. Such a high current and long counting times allow very low detection limits, here estimated to be about 10 ppm for Al, Ca, and Ti, and below 20 ppm for Cr, Mn, and Ni. Mg, Fe, and Si were simultaneously measured on the EDS detector. The JEOL software ZAF method was used for matrix corrections. MongOL sh11-2 olivine reference material was used for major element standardization and for monitoring analytical accuracy and precision during measurements.

We measured the oxygen isotopic compositions of type-I chondrule olivines by SIMS; we targeted nearly all olivine grains within each chondrule and performed multiple analyses within the coarsest zoned olivine grains. We used the CAMECA IMS 1270 E7 at the Centre de Recherches Pétrographiques et Géochimiques (CRPG-CNRS, Nancy, France). $^{16}O^-$, $^{17}O^-$, and $^{18}O^-$ ions produced by a Cs^+ primary ion beam (~10 μm, ~2–2.5 nA, rastered over 5 × 5

μm^2) were measured in multi-collection mode using three Faraday cups (FCs). To remove the interference of $^{16}OH^-$ on the $^{17}O^-$ peak and to maximize the flatness atop the $^{16}O^-$ and $^{18}O^-$ peaks, the entrance and exit slits of the central FC were adjusted to obtain mass resolution power (MRP = $M/\Delta M$) of ~7,000 for $^{17}O^-$. As an additional safeguard against $^{16}OH^-$ interference, a liquid N_2 trap was used to reduce the pressure in the analysis chamber to <1 × 10^{-8} mbar. The two off-axis multicollection FCs, L'2 and H1, were respectively used to measure $^{16}O^-$ and $^{18}O^-$ and were set on exit slit 1 (MRP = 2,500). We used 10^{10} Ω, 10^{12} Ω, and 10^{11} Ω resistors for the L'2 (^{16}O), central (^{17}O), and H1 (^{18}O) FCs, respectively (see Bouden et al. 2021 for further details). A normal-incidence electron gun was used for charge compensation. Total measurement times were 300 s, comprising 120 s of pre-sputtering and 180 s of analysis. Two terrestrial standards, San Carlos olivine and JV1 diopside, were used to define the mass-dependent fractionation line. The instrumental mass fractionation (IMF) of chondrule olivine grains was corrected using San Carlos olivine. To monitor any instrumental drift and to achieve good precision, the San Carlos olivine was analyzed after every 15–20 sample analyses. Typical count rates obtained on San Carlos olivine were 1.0 × 10^9 cps, 4.0 × 10^5 cps, and 2.1 × 10^6 cps for ^{16}O, ^{17}O, and ^{18}O, respectively. All SIMS analytical spots were checked thoroughly by scanning electron microscopy, and any spot near fractures, in the mesostasis, or not completely within olivine grains was excluded from the dataset. Oxygen isotopic compositions are expressed in δ units as $\delta^{17,18}O = [(^{17,18}O/^{16}O)_{sample}/(^{17,18}O/^{16}O)_{V\text{-}SMOW} - 1] \times 1{,}000$ ‰ where V-SMOW refers to the Vienna Standard Mean Ocean Water value. Samples related by mass fractionation to the composition of V-SMOW fall on a line with a slope of 0.52 (defining the Terrestrial Fractionation Line, TFL) whereas mass-independent variations are described $\Delta^{17}O = \delta^{17}O - 0.52 \times \delta^{18}O$ (representing vertical deviations from the TFL in a triple oxygen isotope diagram). Typical 2σ measurement errors,

accounting for internal errors on each measurement and the external reproducibility of the standards, were estimated to be ~0.4 ‰ for $\delta^{18}O$, ~0.7 ‰ for $\delta^{17}O$, and ~0.7 ‰ for $\Delta^{17}O$.

3- Results

Among the 77 Mg-rich type I chondrules examined in two sections of Renazzo and Dar al Gani 574, the seven porphyritic chondrules chosen for detailed characterization were mostly composed of olivine crystals (i.e., porphyritic olivine, PO, chondrules). The selected chondrules had apparent maximum diameters ranging from 300 to 2,000 μm (Figs. 1 & S1–S7). Their olivine is uniformly magnesian, with Mg# spanning from 97.0 to 99.4 (Fig. 2; Table S1). CL maps revealed different textures depending on chondrule size. Chondrules with maximum apparent diameters smaller than ~ 800 μm showed relatively simple textures with inner-chondrule olivine cores depleted in Al and Ti, whereas outer-chondrule olivine crystals were enriched in those elements (Fig. 1B; Table S1), comparable to our results in other CCs (e.g., Jacquet et al. 2021; Marrocchi et al. 2018, 2019). Conversely, larger chondrules show more complex textures where one or several regions may be broadly similar to small chondrules, e.g., chondrule Ch45 in Renazzo whose core is surrounded by large outer shells of Al-Ti-depleted olivine grains (Fig. 1D; Table S1). Olivine minor and trace element concentrations range from 90 to 1,075 ppm TiO_2, 130 to 4,600 ppm Al_2O_3, 1820 to 6,700 ppm CaO, 110 to 4,800 ppm MnO, 1,500 to 7,300 ppm Cr_2O_3, and 20 to 1,200 ppm NiO (Figs. 2–S8, Table S1).

Olivine O isotopic compositions plot along the primitive chondrule mineral line (PCM; Fig. 2A; Ushikubo et al. 2012) with $\delta^{17}O$ and $\delta^{18}O$ values ranging from −12.1 to +1.8 ‰ and from −6.9 to +5.4 ‰, respectively (Fig. 2A, Table S1). Within errors, most of our CR chondrules show constant $\Delta^{17}O$ value (despite variable minor element abundances),

around −2 ‰ or −6 ‰ (Fig. 2; Table S1), both modes (the latter minor) being already known from past CR chondrite literature (e.g., Schrader et al. 2013; Tenner et al. 2015), with $\Delta^{17}O$ anticorrelating with Mg# (Fig. 2D). Since these two populations will be of most importance in the discussion, and for ease of reference, we shall call (i) those type I chondrules (in CR or other CCs) with (host) -4 ‰ $< \Delta^{17}O < -0.5$ ‰ ***"type I-CR"*** (because they comprise most chondrules in CR chondrites) and (ii) those type I chondrules with $\Delta^{17}O < -4$ ‰ ***"type I-CO"*** (as they dominate chondrules in other CCs, in particular CO and CO-like Acfer 094 where the dichotomy has been first identified; Ushikubo et al. 2012; Tenner et al. 2013). By themselves, the names "type I-CR" and "type I-CO" should not be construed to imply that the corresponding chondrule populations are monogenic or indigenous to the parental reservoirs of the eponymous chondrites. Combined with literature data, our results show a systematic relationship between CR chondrule sizes and their $\Delta^{17}O$ (Fig. 3; Schrader et al. 2014; Tenner et al. 2015) with small chondrules being generally ^{16}O-richer than larger ones. The respective average areas (± standard deviation) of type I-CR and type I-CO chondrules are 0.75±0.59 and 0.28±0.15 mm^2. With a corresponding diameter of 0.6 mm, the type I-CO chondrules may thus be closer to CO or CM chondrules (mean diameters of 0.11-0.297 mm and 0.27 mm in the Friedrich et al. (2015) compilation) than say CV (0.69-1.44 mm). However, the values herein are liable to bias in the selection of the chondrules in this and previous studies (e.g. in favor of big chondrules).

The only exception to intrachondrule homogeneity is type I-CR chondrule Ch−16 from Renazzo, with the three olivine grains with $\Delta^{17}O \sim -6$‰ displaying narrower chemical variations than those having $\Delta^{17}O \sim -2$‰ (Fig. S8, Table S1) and being thus identifiable as relict grains (e.g., Marrocchi et al. 2018, 2019; Ushikubo et al. 2012).

4-Discussion

4-1 Relict grains in CR chondrules

In this study, only three grains (out of 200 spot analyses, i.e., 1.5 %), all in Renazzo chondrule Ch-16, were isotopically identifiable as relicts. This is in contrast to the 17 (out of 116 olivine analyses, ~15 %) and 19 relicts (out of 199, ~10 %) previously found in NWA 5958 (C2-ung; Marrocchi et al. 2018) and Kaba (CV3; Marrocchi et al. 2019), respectively. Our results are however in line with an earlier compilation that counted 14 relicts out of 278 analyses (~5 %) in CR chondrites compared to 32 relicts out of 100 analyses (32 %) in CO chondrites (Tenner et al. 2018) —the difference in absolute magnitude being attributable to different search strategies (Piralla et al. 2021). Schrader and Davidson (2017) also noted fewer forsteritic relicts in *type II* chondrules in CR compared to CO (although the former were comparable to CM).

None of the relicts found in this study or in earlier CR literature (Schrader et al. 2013; Tenner et al. 2015) has $\Delta^{17}O$ below −10 ‰, although such ^{16}O-rich compositions made half of Kaba relicts identified by (Marrocchi et al. 2019a). ^{16}O-rich forsteritic relicts in CR chondrites were only reported in the less melted so-called “agglomeratic objects” (Schrader et al. 2018). This is comparable to results in non-carbonaceous chondrites, with (i) no $\Delta^{17}O$ < −10 ‰ olivine being identified in R chondrules (Regnault et al. 2022) and (ii) only 2 out of 17 relicts (out of 649 analyses) reported in LL chondrites (Piralla et al. 2021). Since such ^{16}O-rich isotopic compositions have been linked to refractory inclusions (with $\Delta^{17}O$ around −25 ‰; e.g., Marrocchi et al. 2018, 2019), Regnault et al. 2022 ascribed such paucity in NC chondrites to the rarity of refractory inclusions therein (and in the chondrule precursors) relative to carbonaceous chondrites. The same explanation may be adopted here, as CR

chondrites are depleted in refractory inclusions compared to most other CCs (0.5 vol%; Bryson and Brennecka 2021).

The relict grains of Renazzo chondrule Ch-16 (Figs. S2 & S8) have $\Delta^{17}O \sim -6‰$, similar to the few relict grains previously identified in CR chondrites (Tenner et al. 2015). This isotopic signature is comparable to the minor *type I-CO* chondrule population in CR (Fig. 2; Tenner et al. 2015) and most chondrules in other CCs, *viz.* CM-CV-CO (e.g., Jacquet et al. 2021). The relict grains may thus have been inherited from such chondrules, fragmented or whole, in more or less dusty aggregates that were re-melted in a $\Delta^{17}O \sim -2‰$ reservoir that buffered the O isotopic composition of the host crystals through gas-melt exchange (e.g., Marrocchi et al. 2018, 2019; Schrader et al. 2013).

4.2 Evidence for two generations of CR chondrules

The above relict grain observations indicate that, in CR chondrites, *type I-CO* chondrule formation in a $\Delta^{17}O \sim -6$ ‰ environment predated *type I-CR* chondrule formation in a $\Delta^{17}O \sim -2$ ‰ environment. This is borne out by Al-Mg dating as magnesium-26 excesses (interpreted as ingrowth from then-live aluminium-26) were found in 5 CR chondrules with $\Delta^{17}O$ between −5.3 and −4.2 ‰ (i.e. *type I-CO* chondrules in our parlance) and none in less ^{16}O-rich chondrules (Tenner et al. 2019). These two populations of chondrules are distinct in major element mineral chemistry, with the latter being less magnesian than the others (Schrader et al. 2013; Tenner et al. 2015). A major result of our study is that these two chondrule populations are also texturally distinct (Figs. 1, S1−S7). The *type I-CO* chondrules are small and characterized by textures similar to CM−CV−CO chondrules (Jacquet et al. 2021; Libourel and Portail 2018; Marrocchi et al. 2018, 2019a). Conversely, *type I-CR* chondrules are large and display complex textures (Fig. 1). Taken together, this demonstrates

the existence of two distinct chondrule populations in CR chondrites with small *type I-CO* chondrules being similar to CM–CV–CO chondrules whereas large *type I-CR* chondrules result from their recycling during at least one additional melting episode.

The difference in size may reflect (i) different precursor sizes in their respective formation reservoirs, (ii) different growth rates by droplet collisions during chondrule formation and/or (iii) differential size sorting (Jacquet 2014). In case (i), the precursors of the second-generation chondrules may have comprised whole early-generation chondrules surrounded by dust mantles. Case (ii) would basically cast the large chondrules as "blurred" compound chondrules (e.g., Jacquet 2021), which could explain their complex textures (Fig. 1). Case (iii) could explain the small size of the first generation of chondrules given that small grains drift less rapidly inward than bigger ones (Jacquet et al. 2012). In the latter scenario, the first generation of chondrules could have diffused outward from shorter heliocentric distances or were formed essentially locally, with larger ones being preferentially lost. In addition, the larger size of the *type I-CR* chondrules and/or the lower gas densities at late times could have favored their settling to the midplane (e.g., Jacquet et al. 2012) and the enhancement of the solid/gas ratio inferred to explain their less magnesian compositions (e.g., Schrader et al. 2013; Tenner et al. 2015, 2019).

It is noteworthy that *type I-CR* chondrules are isotopically close (in O, Cr, Ti) to bulk CR chondrites (Schneider et al. 2020). In addition to relict grains, this is further evidence that these chondrules formed out of local CR material, including the earlier generation of chondrules, rather than being an independent population of chondrules that mixed with the early-formed, smaller ones. The isotopic difference between the two original reservoirs may reflect the physical mixing of solid grains and/or ices (Schrader et al. 2014; Tenner et al. 2015) with different origins and oxygen isotopic compositions. However, ^{16}O-poor ices *alone* would not suffice to make the difference, as ^{16}O-richer chondrules appear also ^{54}Cr-poorer

(Schrader et al. 2020). The nature of the material admixed between the two chondrule generations will be discussed more in the upcoming section.

4.3 Reconstructing the original CR reservoir

The evidence for a late generation of chondrules in CR chondrites raises the question of what the CR reservoir looked like prior their formation—this we call the "*original CR reservoir*". According to (Schrader et al. 2014), chondrules make up 64.6 vol% of CR chondrites on average, 96 % of which being type I chondrules (Schrader et al. 2011, 2015). Among the latter, (Tenner et al. 2015) measured 30 chondrules with $\Delta^{17}O > -4$ ‰ and 10 with $\Delta^{17}O < -4$ ‰. If this can be taken as representative of their relative abundances, the *type I-CR* chondrules should comprise a fraction of about $(30/40) \times 0.96 \times 0.646 \approx 0.5$, implying that the final chondrule-forming episode(s) converted about half of the mass in the CR chondrite reservoir into *type I-CR* chondrules. If this reservoir behaved as an essentially closed system (for the nonvolatile portion) until accretion, the present-day fractions of refractory inclusions and *type I-CO* chondrules (0.005 and 0.15, respectively) would only represent half those extant before that final chondrule-formation time. Consequently, the CR chondrite reservoir may have originally contained 1 vol% of refractory inclusions and 30 vol% of *type I-CO* chondrules. Of note, these may be overestimates if some of these components were actually added to the CR reservoir during or after this final chondrule-forming epoch. At any rate, this paints a picture of an original CR reservoir enriched in fine-grained dust and poor in refractory inclusions —more so in either respect than even CM chondrites. Interestingly, CR chondrites are characterized by drastic differences in matrix abundance, ranging from 20 to 70 vol% (Hellmann et al. 2020; Schrader et al. 2011; Schrader

et al. 2014). If correct, our model would thus imply that matrix−rich CRs (e.g., Al Rais and NWA 852) experienced fewer, if any late recycling.

If the CR reservoir was indeed as matrix-rich as envisioned here, this would bring CR back in line with other CCs in isotopic ratios *vs.* modal abundance diagrams (Fig. 4). As noticed by Bryson and Brennecka (2021), the ε^{54}Cr of CR chondrites suggest that a significant fraction of fine-grained matrix with CI-like composition was incorporated into CR chondrites before the last epoch of chondrule formation. Consequently, the original CR reservoir may have been intermediate between CM-CO-CV chondrites and CI. To be more quantitative, we now interpolate compositions intermediate between CO and CI chondrites as binary mixtures between these endmembers (we choose CO as the chondrule-rich endmember because their chondrule sizes may be closest to *type I-CO* chondrules in CR but do not necessarily imply that type I-CO chondrules were produced in the very same reservoir as CO chondrules). Matching the Cr isotopic composition of CR then requires 59 wt% CI dust and 41 wt% CO (using Cr concentrations from Braukmüller et al. 2018 and isotopic data compiled by Hellmann et al. 2020). With CO themselves containing 30 vol% matrix, this would suggest matrix modal abundances of ~70 vol%, in line with our independent estimate above, and comparable to the ~80 wt% appraised on the same basis of Cr isotopic compositions by Bryson and Brennecka (2021). A similar figure would have been obtained from O isotopic compositions: Taking $\Delta^{17}O = -6‰$ for *type I-CO* chondrule precursors (Tenner et al. 2018) and $\Delta^{17}O = +0.5‰$ for the CI-like matrix, the $\Delta^{17}O \sim -2‰$ of *type I-CR* chondrules would be achieved with the incorporation of ~70% of CI-like matrix during chondrule formation. It thus appears that the original CR reservoir was dominated by CI dust (as also assumed in the O isotope/Mg# calculations of Tenner et al. 2015).

However, such a reconstructed original CR reservoir would markedly differ from present-day CR chondrites in bulk chemistry, since the latter are much more devolatilized.

The calculated CO-CI mixture shows "plateau volatile elements" (i.e., elements with T_{50} condensation temperatures between 500 and 800 K) at ~0.7 × CI *vs.* ~0.2 × CI (Cr-normalized) for analyzed CRs (Fig. 5, Braukmüller et al. 2018). This indicates that the last chondrule-forming events incurred a *bulk* loss of volatile elements in the CR reservoir (similar to a suggestion by Bryson and Brennecka, 2021). Importantly, matrix−poor CR chondrites fall on the trend defined by other CCs between the abundances of plateau volatile elements and the mass-fraction of matrix (Hellmann et al. 2020). This implies that, similarly to other CCs, the volatile content of CR chondrites is also controlled by the abundance of matrix (Hellmann et al. 2020). Since the reduction factor of the plateau volatile elements (~3-4; Fig. 5) is greater than that of the matrix abundance between matrix-rich and matrix-poor CRs (~2; Schrader et al. 2014), some matrix-destined dust must have experienced devolatilization as well.

Since Te is one of the plateau volatile elements, this devolatilization could explain why CR chondrites plot off of the δ^{128}Te–ε^{54}Cr mixing line defined by other CCs (Fig. 6; Hellmann et al. 2020). From the Te measurements of Hellmann et al. (2020), the original CR reservoir reconstructed above would have 1.69 ± 0.05 ppm Te and δ^{128}Te of 0.11 ± 0.04 ‰. This correction would align CR chondrites with δ^{128}Te–ε^{54}Cr correlation defined by all other CCs (Fig. 6), thus confirming that significant amounts of CI-like matrix were incorporated into CR chondrules. The (presumably evaporative) loss of Te would have affected its isotopic composition, with δ^{128}Te now lower by 0.2 ‰, possibly because the (incomplete) recondensation would have preferentially involved light isotopes (e.g., Marrocchi et al. 2019b), as seems to be the case for other similarly Te-depleted (and chondrule-rich) CCs (Hellmann et al. 2020). Importantly, this does not affect mass-independent parameters like ε^{54}Cr or Δ^{17}O, which have been used above to reconstruct the original CR reservoir.

4.4 Origin of the peculiar ε^{54}Cr of CR chondrules

The original CR reservoir may thus have consisted of *type I-CO* chondrules, other high-temperature components (e.g., CAIs), cogenetic dust, and more freshly admixed (and dominant) dust of CI composition. The precursors of individual *type I-CR* chondrules would have comprised stochastically varying proportions of these components (plus early formed type I-CR chondrules themselves if they formed in several episodes). Now, the high-temperature components other than *type I-CO* chondrules would have been largely subdominant. In addition, the dust cogenetic with them would have been likely fairly close to CI in chemistry, judging from the matrix of other CCs (e.g., Bland et al. 2005; van Kooten et al. 2019), and would not affect much the CI composition of late-injected unfractionated CI dust. Consequently, the *type I-CR* chondrule precursors could be approximated as binary mixtures between *type I-CO* chondrules and CI-like dust (Fig. 7).

Type-I CR chondrules have specific ε^{54}Cr values of 1.44 ± 0.14 (van Kooten et al. 2016; Olsen et al. 2016; Schneider et al. 2020) that are higher on average and far less variable than those characterizing CM-CV-CO chondrules (ε^{54}Cr of ~ 0.66 ± 0.49; van Kooten et al. 2020; Olsen et al. 2016; Schneider et al. 2020; Williams et al. 2020; Zhu et al. 2019). The lower variability may be traced back to the paucity of (^{54}Cr-rich) CAIs in CR compared to other CCs, where they could produce a "nugget effect" such as that described by Ebert et al. 2018 for ^{50}Ti. The difference in the *average* isotopic ratios can be accounted for in the framework of the present model by considering that *type I-CR* chondrules result from the mixing of 30 % of *type I-CO* precursors (with ε^{54}Cr of ~ 0.66) with 70 % of CI–like matrix (with ε^{54}Cr ~ 1.56 ± 0.06; Bryson and Brennecka 2021; Trinquier et al. 2007). This produces *type I-CR* chondrules with ε^{54}Cr = 1.31 (Fig. 7), in good agreement with the isotopic compositions reported for CR chondrules (Olsen et al. 2016; Schneider et al. 2020). The

higher Cr concentrations of *type I-CR* chondrules (~ 4000 ppm Cr on average; Schneider et al. 2020) relative to both *type I-CO* chondrules and CI chondrites (~ 2,960 and 2,620 ppm, respectively) also points out again the importance of devolatilization during the formation of *type I-CR* chondrules in CR chondrites. These results support our conclusions that CR chondrites comprise distinct chondrule populations, with small *type I-CO* chondrules similar to CM-CV-CO chondrules and large *type I-CR* chondrules formed by the mixing and melting of CI-like matrix with *type I-CO* chondrules.

4.5 Implications for the timing and location of CR chondrule formation

Based on the Al–Mg systematic, CR chondrules have been suggested to have formed 3.5–4 Ma after the condensation of CAIs, i.e., 1–2 Ma later than chondrules in other chondrite groups (Schrader et al. 2017). However, the chronological significance of Al–Mg data, which is based on the assumed homogenous distribution of ^{26}Al in the disk, is regularly challenged (e.g., Bollard et al. 2017). Therefore, alternative explanations of the low initial ^{26}Al/^{27}Al ratio in CR chondrules include their formation (i) in a ^{26}Al-poor region of the disk, potentially beyond the orbit of Saturn and/or (ii) from thermally unprocessed molecular cloud material (van Kooten et al. 2016, 2020). Nonetheless, U-corrected Pb–Pb dating of individual CR chondrules still make them the youngest, *on average*, among chondrites (except CB, CH; Bollard et al. 2017). Al-Mg dating of CR chondrules evidence ^{26}Al/^{27}Al ratios in *type I-CO* chondrules (i) higher than those in *type I-CR* chondrules and (ii) comparable to those in most CO chondrules (Tenner et al. 2019). In addition, CO chondrites and Acfer 094 contain a minor population of *type I-CR* chondrules (at Δ^{17}O ~ –2‰, like most CR chondrules) whose ^{26}Al/^{27}Al ratios are indistinguishable from their ^{16}O-richer (*type I-CO*) counterparts. This suggests that chondrule formation had already begun in a CR-like reservoir when CO

chondrites accreted (Jacquet et al. 2021), and that this reservoir had the same $^{26}Al/^{27}Al$ ratio as the CO reservoir at that time (type I-CO chondrules themselves may have formed over a protracted interval; e.g. Ushikubo et al. 2013; Schrader et al. 2017; Fukuda et al. 2022). Furthermore, the ^{26}Al ages of CR chondrules are concordant with Hf–W ages (Budde et al. 2018), for which it is well established that ^{182}Hf was homogenously distributed throughout the protoplanetary disk (Kruijer et al. 2014). This thus represents strong evidence for (i) the disk-wide homogenous distribution of ^{26}Al and (ii) the late formation of (most) CR chondrules compared to other CC groups. This is in line with our data showing that recycling processes play a key role in the formation of CR chondrules compared to other CC chondrules.

Was the CR reservoir—wherever it was—peculiar in any respect? We have shown that the peculiar ^{54}Cr isotopic compositions of CR chondrules result from admixtures of CI-like matrix with CM-CV-CO chondrule-like precursors. These had $\Delta^{17}O$ values similar to those of CM-CV-CO chondrules (Figs. 2–3), suggesting that the first generation of CR chondrules formed from a homogenous O isotopic reservoir indistinguishable from them (Marrocchi et al. 2019a; Tenner et al. 2018). What makes CR chondrites unique is largely the existence of an extensive late stage of chondrule recycling. In the mean time, our model suggests that CI-like dust would have flown into their region of formation. This is evidence that CI-like dust is a ubiquitous component of the CC reservoir (Hellmann et al. 2020), although this CI-like dust was not necessarily entirely isotopically uniform. While the Cr, O, Ti isotopic systematics favor an isotopic match with actual CI chondrites, CR chondrites still retain some specificities: (i) H and N are isotopically heavier in the CR clan than in other chondrites (Aleon 2010; Piani et al., 2021) and (ii) CR are enriched in ^{94}Mo relative CI chondrites (Kleine et al. 2020) and somewhat ^{26}Mg-poorer (van Kooten et al. 2021). Consequently, the late CI-like dust that abounded in the CR reservoir was likely somewhat different from our CI chondrites. Thus, the chemically solar CI-like dust probably varied

somewhat isotopically in the disk, though for many isotopic systems (e.g. Cr, Ti, O), such variation was apparently limited.

5. Conclusions

We have combined CL mapping, *in-situ* EMPA and SIMS oxygen isotopic analyses of 7 porphyritic olivine-rich type I chondrules in the Renazzo and Dar al Gani 574 CR chondrites. We found the previously described bimodal distribution in $\Delta^{17}O$, with dominant chondrules with $\Delta^{17}O > -4$ ‰ ("*type I-CR* chondrules") coexisting with chondrules with $\Delta^{17}O < -4$ ‰ ("*type I-CO* chondrules"). Based on our data and the literature, we discovered that *type I-CR* chondrules are on average larger than type I-CO chondrules in CR chondrites. The chondrules are mostly isotopically homogeneous but one *type I-CR* chondrule displayed three *type I-CO*-like relict grains.

We interpret type I-CR chondrules as a second generation of chondrules postdating that of *type I-CO* chondrules. Prior to the formation of *type I-CR* chondrules, the CR reservoir was dominated by fine-grained dust. The isotopic proximity of CR chondrites with CI chondrites suggests that this dust was CI-like in composition. So to a first approximation, the precursors of *type I-CR* chondrules may have been mixtures of earlier *type I-CO* chondrules with CI-like matrix material. Thus, CR chondrites before the last chondrule generation may have largely fit the continuum presented by other carbonaceous chondrites (from matrix-poor CO and CV to matrix-rich CI), if with some isotopic specificities for some elements.

Acknowledgments

Original data from this study are available on the Ordar database: https://doi.org/10.24396/ORDAR-93. Laurette Piani, Christoph Burkhardt, Thorsten Kleine, Jonas Schneider, Fridolin Spitzer, and Elias Wölfer are warmly thanked for fruitful scientific discussions. We thank Devin Schrader and Trevis Tenner for helpful reviews, and Frédéric Moynier for editorial handling. This work was funded by l'Agence Nationale de la Recherche through grant CASSYSS ANR-18-CE31-0010-01 (PI Johan Villeneuve). This is CRPG contribution #2815.

References

Aleon J. 2010. Multiple origins of nitrogen isotopic anomalies in meteorites and comets. *The Astrophysical journal* 722:1342–1351.

Bland P. A., Alard O., Benedix G. K., Kearsley A. T., Menzies O. N., Watt L. E., and Rogers N. W. 2005. Volatile fractionation in the early solar system and chondrule/matrix complementarity. *Proceedings of the National Academy of Sciences of the United States of America* 102:13755–13760.

Bollard J., Connelly J. N., Whitehouse M. J., Pringle E. A., Bonal L., Jørgensen J. K., Nordlund A., Moynier F., and Bizzarro M. 2017. Early formation of planetary building blocks inferred from Pb isotopic ages of chondrules. *Science Advances* 3:e1700407.

Bouden N. et al. 2021. Triple Oxygen Isotope Measurements by Multi-Collector Secondary Ion Mass Spectrometry. *Frontiers in Earth Science* 8: 601169.

Brasser R., and Mojzsis S. J. 2020. The partitioning of the inner and outer Solar System by a structured protoplanetary disk. *Nature Astronomy* 4:492–499.

Braukmüller N., Wombacher F., Hezel D. C., Escoube R., and Münker C. 2018. The chemical composition of carbonaceous chondrites: Implications for volatile element depletion, complementarity and alteration. *Geochimica et Cosmochimica Acta* 239:17–48.

Bryson J. F. J., and Brennecka G. A. 2021. Constraints on Chondrule Generation, Disk Dynamics, and Asteroid Accretion from the Compositions of Carbonaceous Meteorites. *The Astrophysical Journal* 912:163.

Budde G., Kruijer T. S., and Kleine T. 2018. Hf-W chronology of CR chondrites: Implications for the timescales of chondrule formation and the distribution of ^{26}Al in the solar nebula. *Geochimica et Cosmochimica Acta* 222:284–304.

Ebert S., Render J., Brennecka G. A., Burkhardt C., Bischoff A., Gerber S., and Kleine T. 2018. Ti isotopic evidence for a non-CAI refractory component in the inner Solar System. *Earth and Planetary Science Letters* 498:257–265.

Friedrich J. M., Weisberg M. K., Ebel D. S., Biltz A. E., Corbett B. M., Iotzov I. V., Khan W. S. and Wolman M. D. (2015) Chondrule size and related physical properties: A compilation and evaluation of current data across all meteorite groups. Geochemistry 75,

419–443.
Fukuda, K., Tenner, T.J., Kimura, M., Tomioka, N., Siron, G., Ushikubo, T., Chaumard, N., Hertwig, A.T., Kita, N.T., 2022. A temporal shift of chondrule generation from the inner to outer Solar System inferred from oxygen isotopes and Al-Mg chronology of chondrules from primitive CM and CO chondrites. Geochimica et Cosmochimica Acta 322, 194–226.
Harju, E.R., Rubin, A.E., Ahn, I., Choi, B.-G., Ziegler, K., Wasson, J.T., 2014. Progressive aqueous alteration of CR carbonaceous chondrites. Geochimica et Cosmochimica Acta 139, 267–292. https://doi.org/10.1016/j.gca.2014.04.048.
Hellmann J. L., Hopp T., Burkhardt C., and Kleine T. 2020. Origin of volatile element depletion among carbonaceous chondrites. *Earth and Planetary Science Letters* 549:116508.
Jacquet E., Gounelle M., and Fromang S. 2012. On the aerodynamic redistribution of chondrite components in protoplanetary disks. *Icarus* 220:162–173.
Jacquet E. 2014. Transport of solids in protoplanetary disks: Comparing meteorites and astrophysical models. *Comptes Rendus Geoscience* 346:3–12.
Jacquet E., Piralla M., Kersaho P., and Marrocchi Y. 2021. Origin of isolated olivine grains in carbonaceous chondrites. *Meteoritics & Planetary Science* 56:13–33.
Jacquet E. 2021. Collisions and compositional variability in chondrule-forming events. *Geochimica et Cosmochimica Acta* 296:18–37.
Johnson B. C., Minton D. A., Melosh H. J., and Zuber M. T. 2015. Impact jetting as the origin of chondrules. *Nature* 517:339–341.
Kleine T., Budde G., Burkhardt C., Kruijer T. S., Worsham E. A., Morbidelli A., and Nimmo F. 2020. The Non-carbonaceous–Carbonaceous Meteorite Dichotomy. *Space Science Reviews* 216:55.
Kruijer T. S., Kleine T., Fischer-Gödde M., Burkhardt C., and Wieler R. 2014. Nucleosynthetic W isotope anomalies and the Hf–W chronometry of Ca–Al-rich inclusions. *Earth and Planetary Science Letters* 403:317–327.
Kruijer T. S., Burkhardt C., Budde G., and Kleine T. 2017. Age of Jupiter inferred from the distinct genetics and formation times of meteorites. *Proceedings of the National Academy of Sciences* 201704461.
Libourel G., and Portail M. 2018. Chondrules as direct thermochemical sensors of solar protoplanetary disk gas. *Science Advances* 4:eaar3321-32.
Lichtenberg T., Drażkowska J., Schönbächler M., Golabek G. J., and Hands T. O. 2021. Bifurcation of planetary building blocks during Solar System formation. *Science* 371:365–370.
Marrocchi Y., Villeneuve J., Batanova V., Piani L., and Jacquet E. 2018. Oxygen isotopic diversity of chondrule precursors and the nebular origin of chondrules. *Earth and Planetary Science Letters* 496:132–141.
Marrocchi Y., Euverte R., Villeneuve J., Batanova V., Welsch B., Ferrière L., and Jacquet E. 2019a. Formation of CV chondrules by recycling of amoeboid olivine aggregate-like precursors. *Geochimica et Cosmochimica Acta* 247:121–141.
Marrocchi Y., Villeneuve J., Jacquet E., Piralla M., and Chaussidon M. 2019b. Rapid condensation of the first Solar System solids. *Proceedings of the National Academy of Sciences of the United States of America* 116:23461–23466.
Olsen M. B., Wielandt D., Schiller M., Van Kooten E. M. M. E., and Bizzarro M. 2016. Magnesium and ^{54}Cr isotope compositions of carbonaceous chondrite chondrules – Insights into early disk processes. *Geochimica et Cosmochimica Acta* 191:118–138.
Piani L., Marrocchi Y., Vacher L. G., Yurimoto H. and Bizzarro M. (2021) Origin of hydrogen isotopic variations in chondritic water and organics. Earth and Planetary Science Letters 567, 117008.

570 Pinto G. A., Marrocchi Y., Morbidelli A., Charnoz S., Varela M. E., Soto K., Martinez R.,
571 and Olivares F. 2021. Constraints on Planetesimal Accretion Inferred from Particle-size
572 Distribution in CO Chondrites. *The Astrophysical Journal Letters* 917: L25.
573 Piralla M., Villeneuve J., Batanova V., Jacquet E., and Marrocchi Y. 2021. Conditions of
574 chondrule formation in ordinary chondrites. *Geochimica et Cosmochimica Acta* 313:295–
575 312.
576 Regnault M., Marrocchi Y., Piralla M., Villeneuve J., Batanova V., Schnuriger N., and
577 Jacquet E. 2022. Oxygen isotope systematics of chondrules in Rumuruti chondrites:
578 Formation conditions and genetic link with ordinary chondrites. *Meteoritics & Planetary*
579 *Science* 57:122–135.
580 Ribas Á., Bouy H., and Merín B. 2015. Protoplanetary disk lifetimes vs stellar mass and
581 possible implications for giant planet populations. *Astronomy & Astrophysics* 576:A52.
582 Schneider J. M., Burkhardt C., Marrocchi Y., Brennecka G. A., and Kleine T. 2020. Early
583 evolution of the solar accretion disk inferred from Cr-Ti-O isotopes in individual
584 chondrules. *Earth and Planetary Science Letters* 551:116585.
585 Schrader, D.L., Franchi, I.A., Connolly Jr, H.C., Greenwood, R.C., Lauretta, D.S., Gibson,
586 J.M., 2011. The formation and alteration of the Renazzo-like carbonaceous chondrites I:
587 Implications of bulk-oxygen isotopic composition. Geochim. Cosmochim. Acta 75, 308–
588 325. https://doi.org/10.1016/j.gca.2010.09.028.
589 Schrader D. L., Connolly Jr H. C., Lauretta D. S., Nagashima K., Huss G. R., Davidson J.,
590 and Domanik K. J. 2013. The formation and alteration of the Renazzo-like carbonaceous
591 chondrites II: Linking O-isotope composition and oxidation state of chondrule olivine.
592 *Geochimica et Cosmochimica Acta* 101:302–327.
593 Schrader D. L., Nagashima K., Krot A. N., Ogliore R. C., and Hellebrand E. 2014. Variations
594 in the O-isotope composition of gas during the formation of chondrules from the CR
595 chondrites. *Geochimica et Cosmochimica Acta* 132:50–74.
596 Schrader, D.L., Connolly Jr, H.C., Lauretta, D.S., Zega, T.J., Davidson, J., Domanik, K.J.,
597 2015. The formation and alteration of the Renazzo-like carbonaceous chondrites III:
598 Toward understanding the genesis of ferromagnesian chondrules. Meteorit Planet. Sci. 50,
599 15–50. https://doi.org/10.1111/maps.12402
600 Schrader, D.L., Davidson, J., 2017. CM and CO chondrites: A common parent body or
601 asteroidal neighbors? Insights from chondrule silicates. Geochim. Cosmochim. Acta 214,
602 157–171. https://doi.org/10.1016/j.gca.2017.07.031
603 Schrader D. L., Nagashima K., Krot A. N., Ogliore R. C., Yin Q., Amelin Y., Stirling C. H.,
604 and Kaltenbach A. 2017. Distribution of ^{26}Al in the CR chondrite chondrule-forming
605 region of the protoplanetary disk. *Geochimica et Cosmochimica Acta* 201:275–302.
606 Schrader D. L., Nagashima K., Waitukaitis S. R., Davidson J., McCoy T. J., Connolly H. C.,
607 and Lauretta D. S. 2018. The retention of dust in protoplanetary disks: Evidence from
608 agglomeratic olivine chondrules from the outer Solar System. *Geochimica et*
609 *Cosmochimica Acta* 223:405–421.
610 Schrader D. L., Nagashima K., Davidson J., McCoy T. J., Ogliore R. C., and Fu R. R. 2020.
611 Outward migration of chondrule fragments in the early Solar System: O-isotopic evidence
612 for rocky material crossing the Jupiter Gap? *Geochimica et Cosmochimica Acta* 282:133–
613 155.
614 Tenner, T.J., Ushikubo, T., Kurahashi, E., Kita, N.T., Nagahara, H., 2013. Oxygen isotope
615 systematics of chondrule phenocrysts from the CO3.0 chondrite Yamato 81020: Evidence
616 for two distinct oxygen isotope reservoirs. Geochim. Cosmochim. Acta 102, 226–245.
617 https://doi.org/10.1016/j.gca.2012.10.034
618 Tenner T. J., Nakashima D., Ushikubo T., Kita N. T., and Weisberg M. K. 2015. Oxygen
619 isotope ratios of FeO-poor chondrules in CR3 chondrites: Influence of dust enrichment and

620 H_2O during chondrule formation. *Geochimica et Cosmochimica Acta* 148:228–250.
621 Tenner T. J., Ushikubo T., Nakashima D., Schrader D. L., Weisberg M. K., Kimura M. and
622 Kita N. T. (2018) Oxygen isotope characteristics of chondrules from recent studies by
623 secondary ion mass spectrometry. In Chondrules (eds. S. S. Russell, H. C. Connolly and A.
624 N. Krot). Cambridge University Press, pp. 196–246.
625 Tenner T. J., Nakashima D., Ushikubo T., Tomioka N., Kimura M., Weisberg M. K., and Kita
626 N. T. 2019. Extended chondrule formation intervals in distinct physicochemical
627 environments: Evidence from Al-Mg isotope systematics of CR chondrite chondrules with
628 unaltered plagioclase. *Geochimica et Cosmochimica Acta* 260:133–160.
629 Trinquier A., Birck J., and Allegre C. J. 2007. Widespread ^{54}Cr Heterogeneity in the Inner
630 Solar System. *The Astrophysical Journal* 655:1179–1185.
631 Ushikubo T., Kimura M., Kita N. T., and Valley J. W. 2012. Primordial oxygen isotope
632 reservoirs of the solar nebula recorded in chondrules in Acfer 094 carbonaceous chondrite.
633 *Geochimica et Cosmochimica Acta* 90:242–264.
634 Vacher L. G., Piani L., Rigaudier T., Thomassin D., Florin G., Piralla M., and Marrocchi Y.
635 2020. Hydrogen in chondrites: Influence of parent body alteration and atmospheric
636 contamination on primordial components. *Geochimica et Cosmochimica Acta* 281:53–66.
637 van Kooten E. M. M. E. et al. 2016. Isotopic evidence for primordial molecular cloud material
638 in metal-rich carbonaceous chondrites. *Proceedings of the National Academy of Sciences*
639 *of the United States of America* 113:2011–2016.
640 van Kooten E. M. M. E., Moynier F., and Agranier A. 2019. A unifying model for the
641 accretion of chondrules and matrix. *Proceedings of the National Academy of Sciences*
642 116:18860–18866.
643 van Kooten E. M. M., Cavalcante L., Wielandt D., and Bizzarro M. 2020. The role of Bells in
644 the continuous accretion between the CM and CR chondrite reservoirs. *Meteoritics &*
645 *Planetary Science* 55:575–590.
646 van Kooten E., Schiller M., Moynier F., Johansen A., Haugbølle T., and Bizzarro M. 2021.
647 Hybrid Accretion of Carbonaceous Chondrites by Radial Transport across the Jupiter
648 Barrier. *The Astrophysical Journal* 910:70.
649 Williams C. D., Sanborn M. E., Defouilloy C., Yin Q.-Z., Kita N. T., Ebel D. S., Yamakawa
650 A., and Yamashita K. 2020. Chondrules reveal large-scale outward transport of inner Solar
651 System materials in the protoplanetary disk. *Proceedings of the National Academy of*
652 *Sciences* 117:23426–23435.
653 Zhao B. et al. 2020. Formation and Evolution of Disks around Young Stellar Objects. *Space*
654 *Science Reviews* 216:43.
655 Zhu K., Liu J., Moynier F., Qin L., Alexander C. M. O., and He Y. 2019. Chromium Isotopic
656 Evidence for an Early Formation of Chondrules from the Ornans CO Chondrite. *The*
657 *Astrophysical journal* 873:82.
658 Zhu K., Moynier F., Schiller M., and Bizzarro M. 2020. Dating and Tracing the Origin of
659 Enstatite Chondrite Chondrules with Cr Isotopes. *The Astrophysical Journal* 894:L26.
660 Zhu (朱柯) K., Moynier F., Schiller M., Alexander C. M. O., Barrat J.-A., Bischoff A., and
661 Bizzarro M. 2021. Mass-independent and mass-dependent Cr isotopic composition of the
662 Rumuruti (R) chondrites: Implications for their origin and planet formation. *Geochimica et*
663 *Cosmochimica Acta* 293:598–609.
664
665
666
667

Figure caption

Fig. 1. (A, C) Back-scattered electron images of type-I PO chondrules Ch-78 and Ch-45, respectively, in CR2 Renazzo. Bright spots are metal beads. (B, D) Cathodoluminescence maps of the same respective chondrules revealing their internal structures. Chondrule Ch-78 shows textures typical of CM-CV-CO chondrules, with inner olivine grains that are depleted in trace elements and surrounded by larger, outer olivine crystals that are enriched in trace elements. Conversely, chondrule Ch-45 is larger and displays a more complex texture; its central part is enriched in trace elements and surrounded by large outer shells of olivine grains depleted in trace elements.

Fig. 2. (A) Triple oxygen isotope plot of the olivine crystals in the seven analyzed CR chondrules. The data show mass-independent variations plotting along the Primary Chondrule Mineral (PCM) line. The Terrestrial Fractionation Line (TFL) is shown for reference. (B, C) Incompatible element concentrations (Al and Ti, respectively) plotted against O isotopic composition ($\Delta^{17}O$), revealing variations in minor element abundances at constant $\Delta^{17}O$ values. The only exception is chondrule Ch-16 in Renazzo, which shows internal, mass-independent O isotopic heterogeneity (see Fig. 5). (D) Olivine Fo content (=100 × Mg/[Mg + Fe]) as a function of $\Delta^{17}O$.

Fig. 3. Oxygen isotopic compositions of CR type I chondrules as a function of their sizes. Small CR chondrules have $\Delta^{17}O$ values similar to those reported for CM-CV-CO chondrules, whereas large CR chondrules are enriched in $^{17,18}O$. Data are from this study (red points) and previous studies (open circles; (Schrader et al. 2014; Tenner et al. 2015). Fragmented

chondrules are excluded. An arbitrary error of 20% was ascribed to the calculated areas due to sectioning effects.

Fig. 4. $\Delta^{17}O$, $\varepsilon^{50}Ti$ and $\varepsilon^{54}Cr$ as a function of the % of matrix (vol%) for all carbonanceous chondrites, including CRs. The reconstructed CR based on the mixing between 30 % of CO-like chondrules and 70 % of CI)-like dust is also reported.

Fig. 5. The $\delta^{128/126}Te$ vs. $\varepsilon^{54}Cr$ trend is established from the compositions of all carbonaceous chondrites (*30*, and references therein) except CRs, which deviate from the trend. The blue data point represents CR chondrite compositions after correction for the recycling of CI-like matrix during their formation (see Supplementary Text).

Fig. 6. CI and Cr-normalized concentrations of whole-rock chondrites for different elements as a function of their Lodders (2003) half-condensation temperature. CR chondrites are compared to a "reconstructed CR" deemed to represent the original CR reservoir (prior to the last generation of chondrules), by considering a mixture between CO and CI chondrites matching the CR Cr isotopic composition. This shows that the last generation of chondrules incurred bulk volatile loss. CM are also compared to "reconstructed CM" calculated on the same basis as a test of the accuracy of the reconstruction in the absence of such a second generation. Chondrite bulk compositions taken from Braukmüller et al. (2018).

Fig. 7. Cartoon of the suggested formation scenario of CR chondrule. An early generation of type I-CO chondrules is hypothesized to mix with dust, some cogenetic, some unrelated and unfractionated, with a CI-like composition. A second melting episode (or sequence of melting episodes) causes the formation of type I-CR chondrules, with loss of volatile elements.

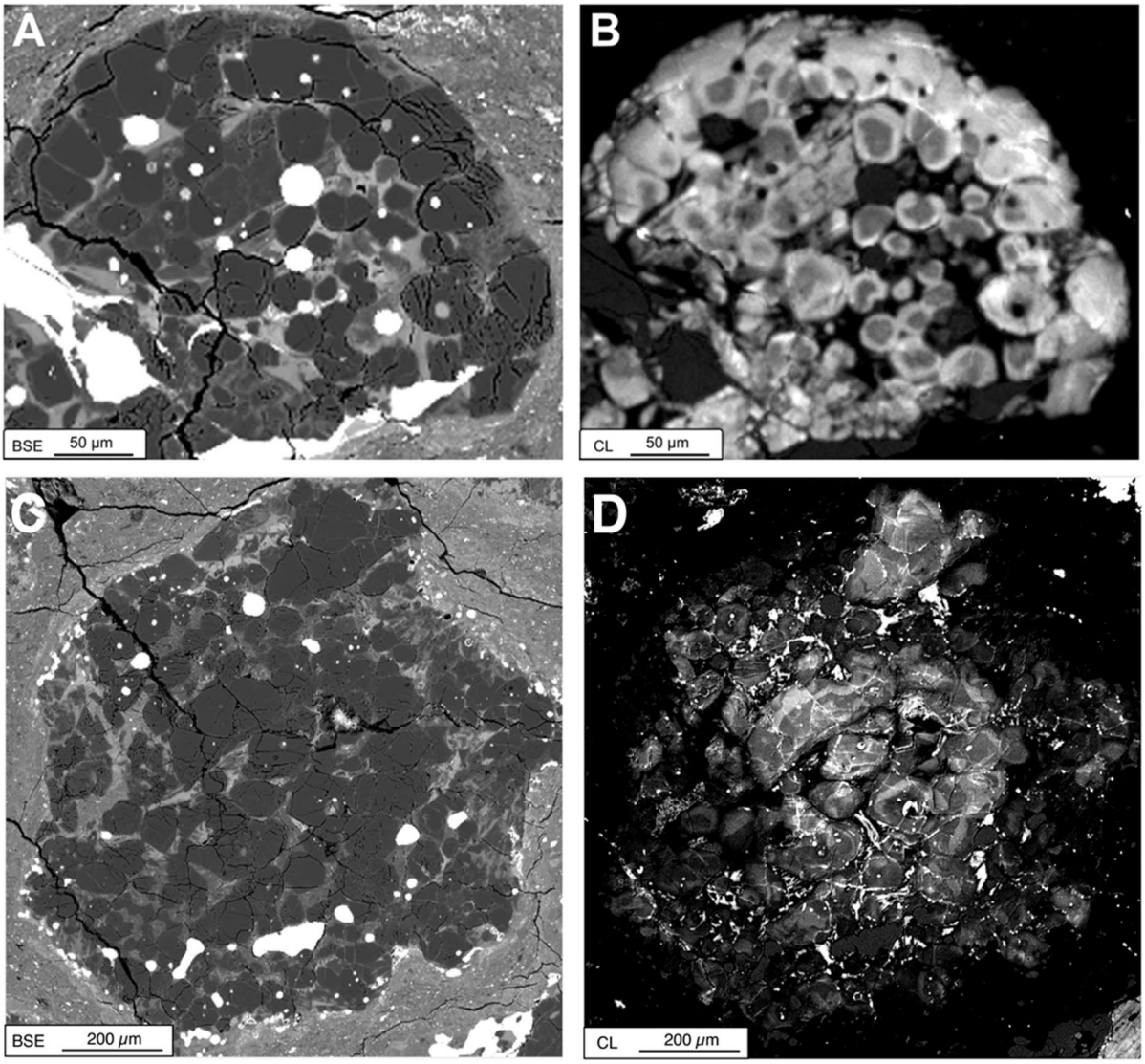

Fig. 1

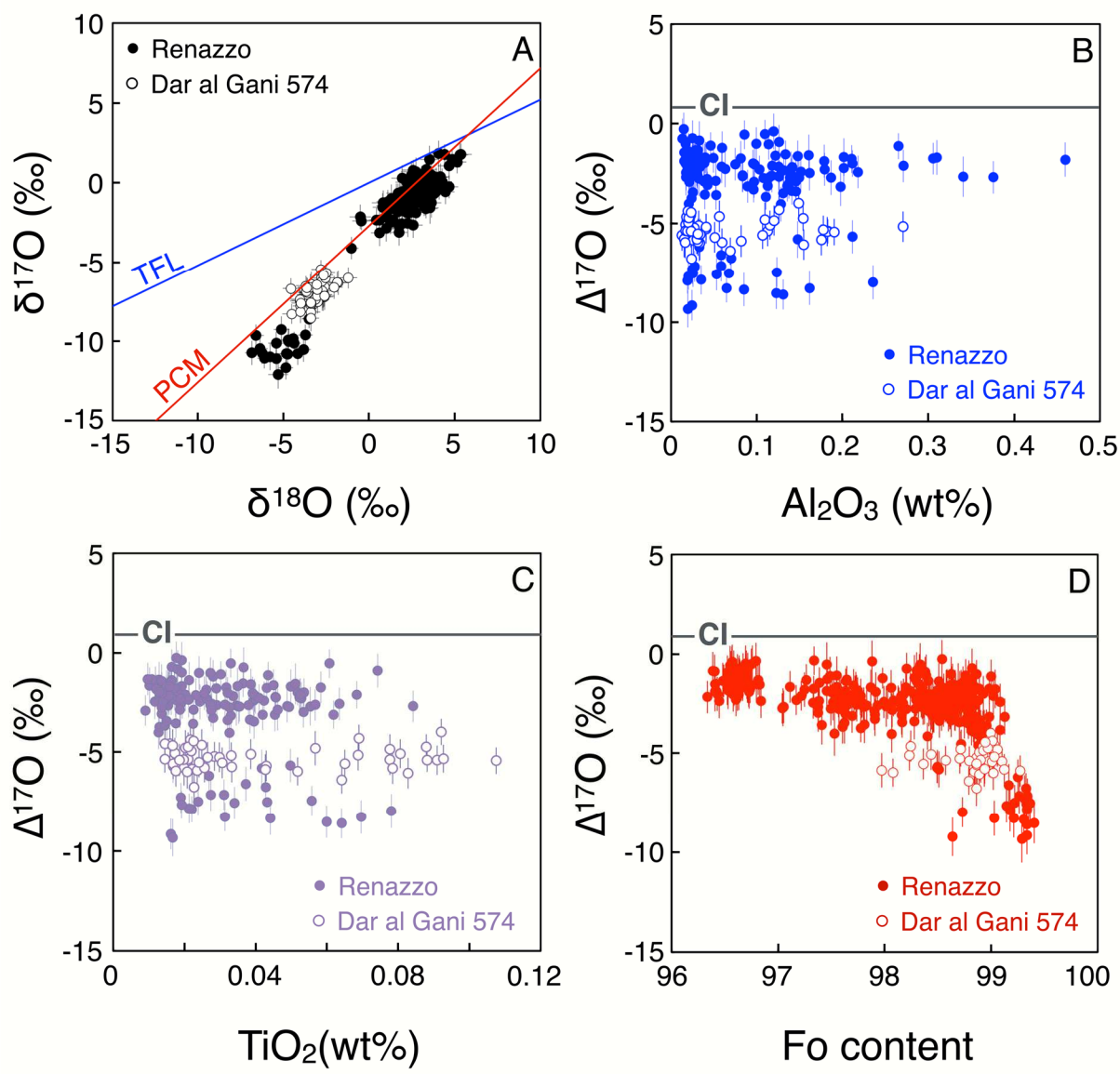
A
Renazzo
Dar al Gani 574
TFL
PCM
δ17O (‰)
δ18O (‰)
B
CI
Renazzo
Dar al Gani 574
Δ17O (‰)
Al2O3 (wt%)
C
CI
Renazzo
Dar al Gani 574
Δ17O (‰)
TiO2(wt%)
D
CI
Renazzo
Dar al Gani 574
Δ17O (‰)
Fo content

Fig. 2

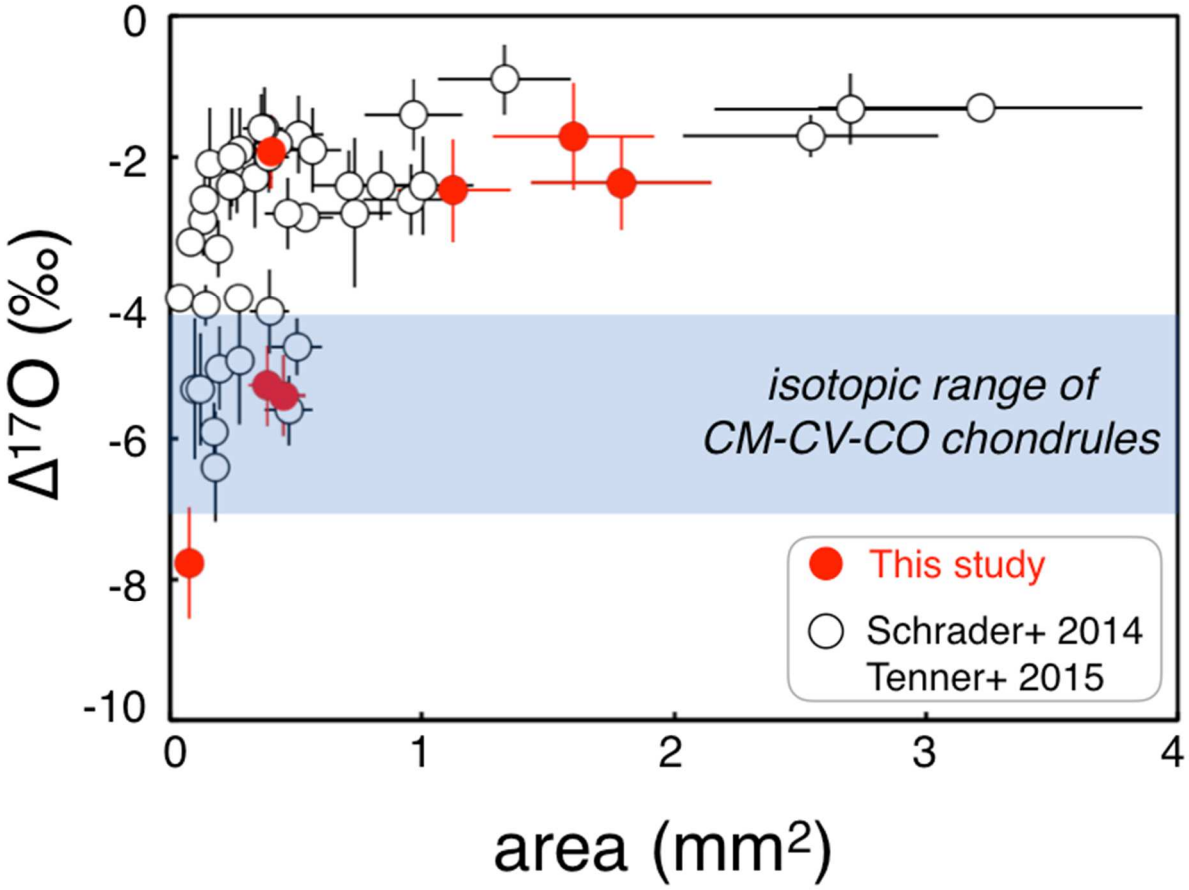

748
749
750 **Fig. 3**
751
752
753

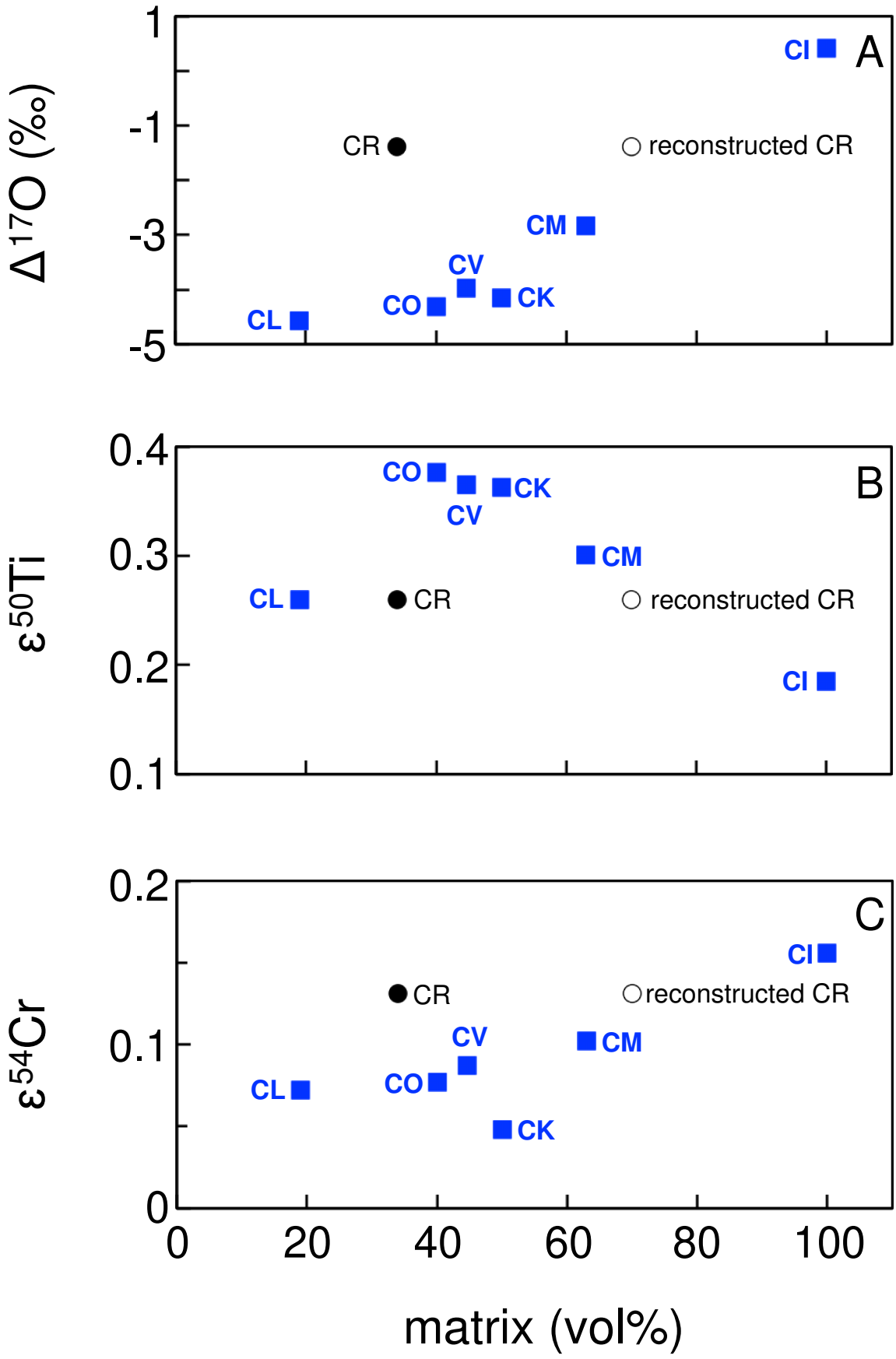
A
B
C
CI
CR
reconstructed CR
CM
CV
CO
CK
CL
Δ17O (‰)
ε50Ti
ε54Cr
matrix (vol%)
1
-1
-3
-5
0.4
0.3
0.2
0.1
0
0
20
40
60
80
100

754
755

Fig. 4

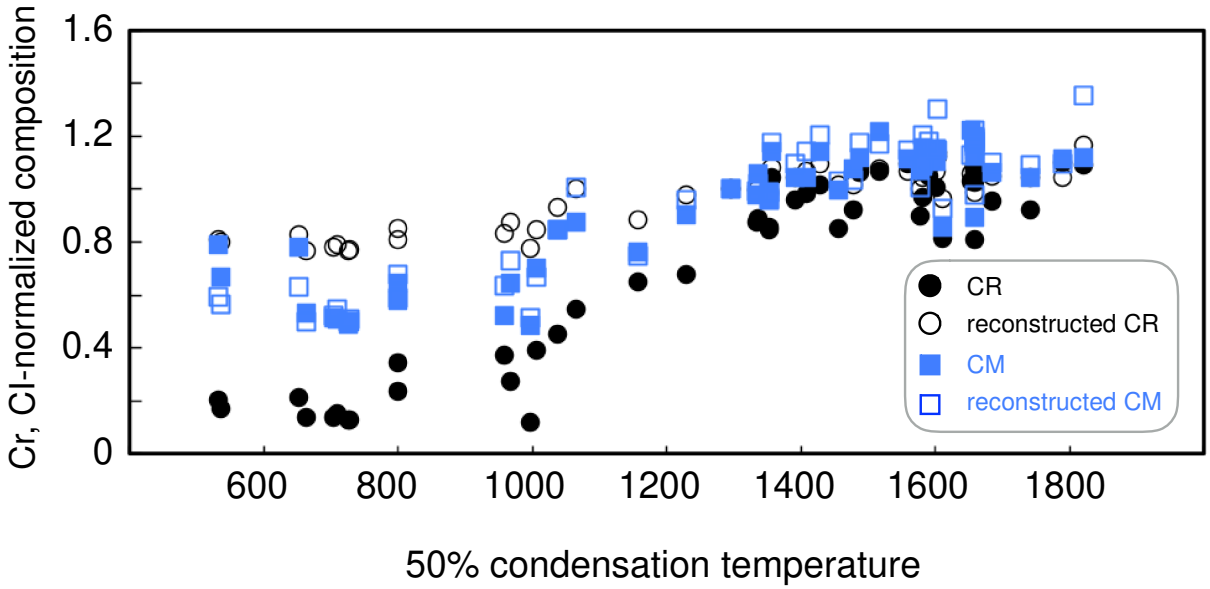
Cr, CI-normalized composition
1.6
1.2
0.8
0.4
0
600
800
1000
1200
1400
1600
1800
50% condensation temperature
CR
reconstructed CR
CM
reconstructed CM

Fig. 5

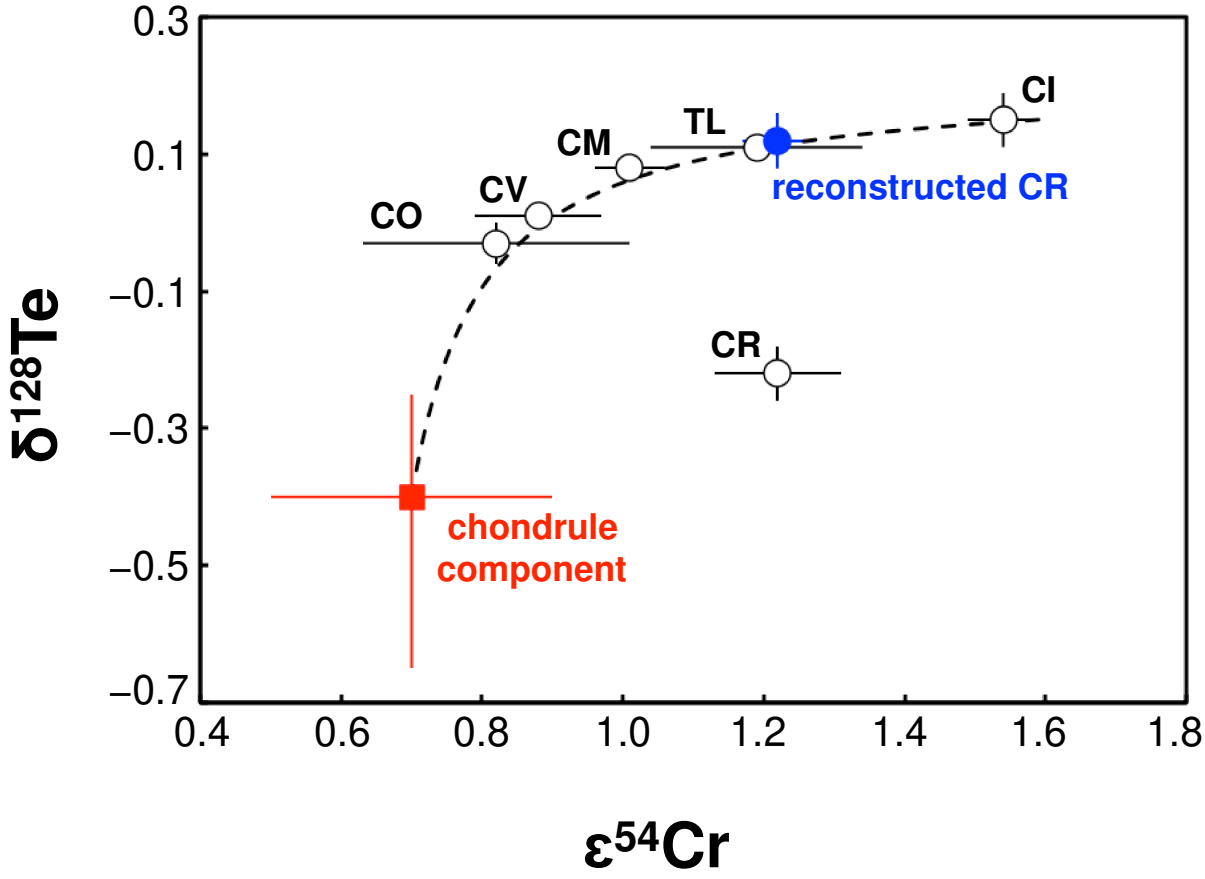
0.3
0.1
−0.1
−0.3
−0.5
−0.7
0.4
0.6
0.8
1.0
1.2
1.4
1.6
1.8
δ128Te
ε54Cr
CI
TL
CM
CV
CO
CR
reconstructed CR
chondrule
component

Fig. 6

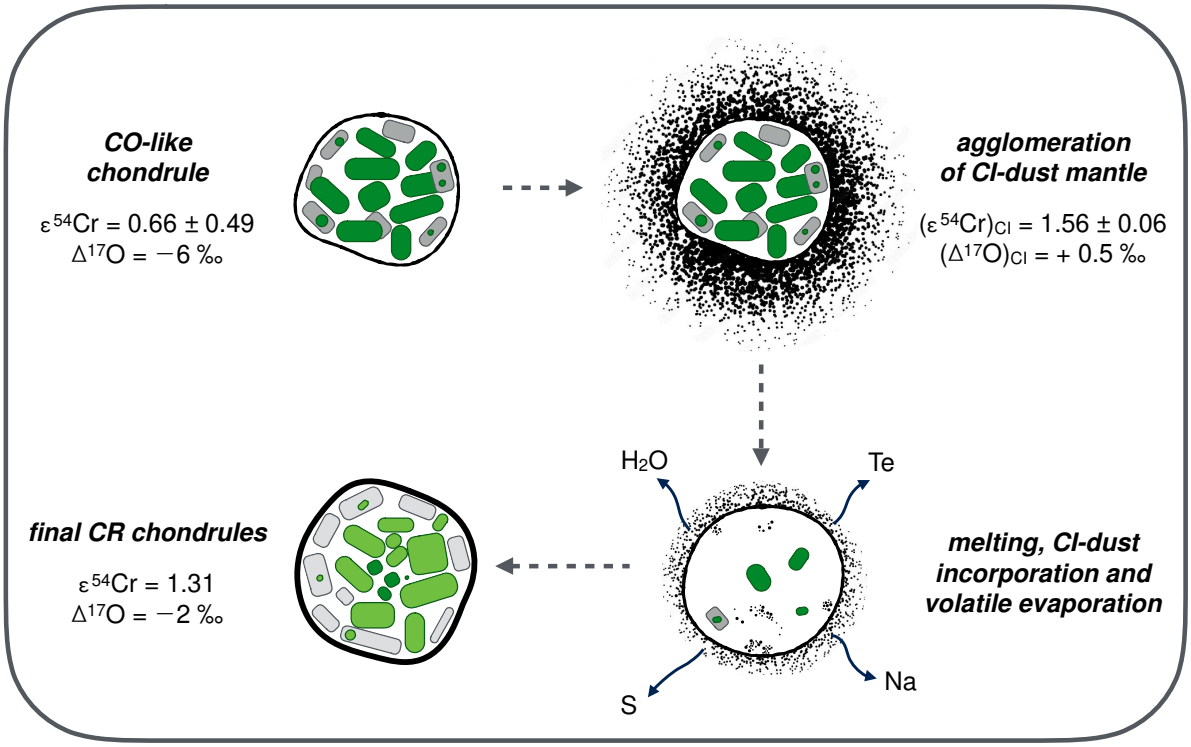
CO-like chondrule
ε54Cr = 0.66 ± 0.49
Δ17O = −6 ‰
agglomeration of CI-dust mantle
(ε54Cr)CI = 1.56 ± 0.06
(Δ17O)CI = + 0.5 ‰
H2O
Te
melting, CI-dust incorporation and volatile evaporation
Na
S
final CR chondrules
ε54Cr = 1.31
Δ17O = −2 ‰

Fig. 7